Appl. Phys. B 87, 355–362 (2007)
DOI: 10.1007/s00340-007-2595-9

Applied Physics B
Lasers and Optics

J.H. ROHLING[1]
J. SHEN[1,✉]
C. WANG[2]
J. ZHOU[1]
C.E. GU[1]

Determination of binary diffusion coefficients of gases using photothermal deflection technique

[1] National Research Council of Canada, Institute for Fuel Cell Innovation, 4250 Wesbrook, Vancouver, British Columbia V6T 1W5, Canada
[2] Institute of Modern Optical Technologies, Suzhou University, Suzhou, Jiangsu 215006, P.R. China

Received: 25 September 2006/
Revised version: 22 January 2007
Published online: 24 March 2007 •

ABSTRACT A photothermal deflection (PD) technique was applied to measure the binary diffusion coefficients of various gases (CO_2–N_2, CO_2–O_2, N_2–He, O_2–He, and CO_2–He). With an in-house-made Loschmidt diffusion cell, a transverse PD system was employed to measure the time-resolved PD signal associated with the variation of the thermal diffusivity and the temperature coefficient of the refractive index of the gas mixture during the diffusion. The concentration evolution of the gas mixture was deduced from the PD amplitude and phase signals based on our diffraction PD model and was processed using two mass-diffusion models explored in this work for both short- and long-time diffusions to find the diffusion coefficient. An optical fiber oxygen sensor was also used to measure the concentration changes of the mixtures with oxygen. Experimental results demonstrated that the binary diffusion coefficients precisely measured with the PD technique were in agreement with the literature values. Moreover, the PD technique can measure the diffusion coefficients of various gas mixtures with both short- and long-time diffusions. In contrast, the oxygen sensor is only suitable for the long-time diffusion measurements of the gas mixtures with oxygen.

PACS 78.20.Nv; 51.20.+d

1 Introduction

Photothermal techniques are measurement schemes that monitor the thermal effects of incident radiation [1, 2]. While processes such as photochemical transformation and reemission of radiation may compete for a share of the excitation energy, a portion of the incident energy is converted into heat in the illuminated substance by a nonradiative deexcitation process. The heating can cause a number of different effects, which provide the detection mechanisms, including temperature rise, surface deformation, infrared emission, and gradients of optical refractive index.

Photothermal deflection (PD) techniques measure the influence of the temperature change on the optical refractive index of the medium in contact with an illuminated solid substance (solid sample) or on the optical refractive index of the solid sample itself. For instance, in a transverse PD scheme, a gradient of the optical refractive index (mirage region) in the medium is induced by a temperature gradient from the sample surface to the medium, due to the absorbed excitation laser energy by the solid sample. A Gaussian probe beam, parallel to the solid sample with a distance x between the solid sample surface and the probe-beam axis, probes the gradient of the optical refractive index in the medium, resulting in the deflection and the diffraction of the probe beam [3]. Henceforth, the medium is named a deflecting medium.

Since the first reported work in 1980 [4], the PD techniques have been widely employed for nondestructive characterization of solid materials, because of the high sensitivity, versatility, and remote (noncontact to its detection system) nature of the PD techniques [1–3, 5–9]. The deflection of the probe beam is not only sensitive to the optical and thermophysical properties of the solid sample, but also dependent on these properties of the deflecting medium. As a result, the PD techniques have also been employed in the study of gases as deflecting media in PD experiments, such as trace-gas detection [10], in situ environmental monitoring and chemical analysis [11], species-selective detection in gas chromatography [12], the observations of laser cooling by resonant energy transfer in CO_2–N_2 mixtures [13], and the measurements of the thermal diffusivities of gases and binary gas mixtures [14–16]. After a precise determination of the distance x between the solid sample and the probe beam in a transverse PD experimental setup, we recently measured the values of the thermal diffusivity α_g and the temperature coefficient of the refractive index dn/dT of three pure gases (O_2, N_2, and CO_2). We also investigated the dependence of α_g and dn/dT of a binary gas mixture, i.e. CO_2–N_2 or CO_2–O_2, on the gas concentration of O_2 or N_2 [16]. We found that the values of α_g and dn/dT changing with concentration could be explained by thermodynamic theory and the Lorentz–Lorenz formula, respectively. Therefore, the PD amplitude and phase signals could be expressed in terms of the composition of the binary gas mixture. This concentration dependence might be used for the real-time monitoring of the gas concentration in a binary gas mixture for various applications. One of the possible applications could be the determination of a binary diffusion coefficient of a gas.

Reliable data on binary diffusion coefficients of gases is of great interest for engineering, environmental, and theoretical applications [17–20]. For example, a gas diffusion layer

✉ Fax: +1-604-221-3001, E-mail: jun.shen@nrc.gc.ca

(GDL) is one of the most important components of a proton-exchange-membrane fuel cell, and an effective gas (usually O_2) diffusion coefficient of the GDL is one of its key properties. A reliable diffusion coefficient of the gas is essential for the theoretical calculation of the effective gas diffusion coefficient. The closed-tube method with a Loschmidt cell is one of the most reliable methods to determine binary diffusion coefficients of gases [20, 21]. With the information of the gas-concentration evolution in the cell due to diffusion, the binary diffusion coefficient can be deduced by means of a proper theoretical model of the gas diffusion.

The concentration evolution usually can be monitored using a gas sensor. However, a gas sensor is usually sensitive only to one particular gas, and the measurements of the binary diffusion coefficients of different gases need various sensors. In addition, some sensors have degradation problems. For optical methods to detect the concentration change, there is no such limitation. Using a holograph interferometric technique, Baranski et al. [20] measured the binary diffusion coefficient of an argon–propane mixture. These two gases formed an ideal binary mixture for this method because of their similar molar masses and densities in addition to their sufficiently different refractive indices. Detecting the gas-concentration change of a binary gas mixture in a Loschmidt cell via the sensing of the PD signal variation because of the changes of α_g and dn/dT of the gas mixture, in this work we measured binary diffusion coefficients using the transverse PD technique. The binary gas mixtures experimentally investigated in this work were CO_2–N_2, CO_2–O_2, N_2–He, O_2–He, and CO_2–He. The time-resolved curves of the concentration changes were fitted to two theoretical diffusion models for long- and short-time diffusions, respectively, to determine the binary gas diffusion coefficients. The binary gas diffusion coefficients thus measured for both long- and short-time diffusions were found to be in good agreement with the literature values. Also, a commercial fiber-optical oxygen sensor was integrated into the Loschmidt cell to determine the binary gas diffusion coefficients for O_2–N_2 and CO_2–O_2. For the long-time diffusion, the results obtained with the oxygen sensor were found in good agreement with the literature values and with the result of CO_2–O_2 using the PD technique. However, for the short-time diffusion, the results with the oxygen sensor differed from the literature values significantly. Our experimental results demonstrated the advantages of the determination of binary diffusion coefficients using the PD technique in terms of the suitability for different gases as well as the reliability and precision for both long- and short-time diffusions.

2 Theory

2.1 *Gas diffusion*

Diffusion is the process by which matter is transported from one part of a system to another as a result of random molecular motions [22]. If the diffusion coefficient D in $m^2\,s^{-1}$ is constant, Fick's second law of diffusion describes the one-dimensional diffusion as

$$\frac{\partial \eta_2}{\partial t} = D\frac{\partial^2 \eta_2}{\partial z^2}\,. \tag{1}$$

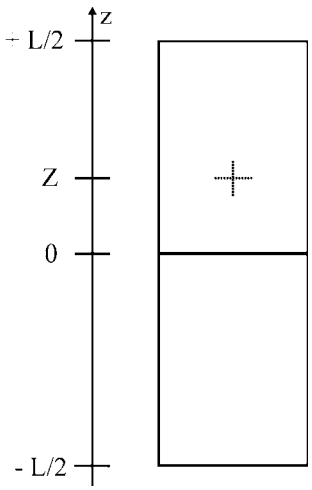

FIGURE 1 A schematic diagram of a Loschmidt cell consisting of two chambers: bottom and top ones

Here η_2 stands for the concentration of species 2. Figure 1 is a schematic diagram of a Loschmidt cell that consists of two chambers. In this work the top and bottom chambers were initially filled with two pure gases: gas (species 1) and gas 2 (species 2), respectively. When these two chambers are connected at $t = 0$, the diffusion starts. One can solve (1) with the following initial and boundary conditions:

$$\eta_2 = \eta_2^{\mathrm{b}} \quad (-L/2 \le z < 0\,,\ t = 0)\,, \tag{2}$$

$$\eta_2 = \eta_2^{\mathrm{t}} \quad (0 < z \le +L/2\,,\ t = 0)\,, \tag{3}$$

$$\left(\frac{\partial \eta_2}{\partial z}\right)_{z=\pm L/2} = 0 \quad (t > 0)\,. \tag{4}$$

Equation (4) is the impermeable boundary condition at $z = \pm L/2$, which means zero flow across the boundaries [22]. η_2^{b} and η_2^{t} are the concentrations of gas 2 at $t = 0$ in the bottom and top chambers, respectively. In this work η_2^{t} is zero. The solution can be expressed as [20]

$$\eta_2(z,t) = \frac{1}{2}\left(\eta_2^{\mathrm{b}} + \eta_2^{\mathrm{t}}\right) - \frac{2\left(\eta_2^{\mathrm{b}} - \eta_2^{\mathrm{t}}\right)}{\pi} \times \sum_{m=0}^{\infty} \frac{\exp\left(-(2m+1)^2\,\pi t/\tau\right)}{2m+1} \sin\left[\frac{(2m+1)\,\pi z}{L}\right]. \tag{5}$$

Here τ is the characteristic diffusion time defined as

$$\tau = \frac{L^2}{\pi D}\,. \tag{6}$$

L in (5) and (6) is the length of the Loschmidt cell shown in Fig. 1.

Equation (5) is a general solution and converges most satisfactorily for large values of time [22]. In practice, sometimes the measurement for a short-time diffusion is convenient and required. For an infinite space and with the initial distribution of gas 2

$$\eta_2 = \eta_2^{\mathrm{b}} \quad (z < 0\,,\ t = 0) \tag{7}$$

and

$$\eta_2 = 0 \quad (z > 0\,,\ t = 0)\,, \tag{8}$$

the solution of (1) can be found in [22]:

$$\eta_2(z,t) = \frac{1}{2}\eta_2^{\mathrm{b}}\mathrm{erfc}\left(\frac{z}{2\sqrt{Dt}}\right). \tag{9}$$

Here $\mathrm{erfc}(x)$ is the complementary error function (also called the error-function complement). Equation (9) is suitable for numerical evaluation at small times [22], during which the diffusion occurs in a finite region. The suitability of (9) for gas diffusion will be discussed later.

2.2 *Photothermal deflection*

Equations (5) and (9) exhibit that with the information of the gas-concentration variation with time, the gas diffusion coefficient can be deduced. This concentration change may be detected using the PD technique [16]. According to the diffraction theory of a transverse PD scheme with the normal deflection, the centroid moment of the probe beam can provide a rigorous measure of the PD [3], and the displacement of the probe-beam centroid can be detected by a position sensor. The fundamental component of the PD signal from the sensor is proportional to the displacement. The amplitude $A(x, f)$ of the PD signal is [16]

$$A(x,f) = -\sqrt{2}\gamma\,|\theta|\,dz_D\frac{1}{\mu_{\mathrm{g}}}\frac{\mathrm{d}n}{\mathrm{d}T}\exp\left(-\frac{x}{\mu_{\mathrm{g}}}\right). \tag{10}$$

Here γ is an instrument factor and θ is the temperature rise on the solid sample surface after the absorption of excitation laser energy. $\mu_{\mathrm{g}} = \sqrt{\alpha_{\mathrm{g}}/\pi f}$ is the thermal diffusion length of the deflection medium, f is the excitation beam modulation frequency, d is the diameter of the excitation beam in the mirage region, and z_D is the distance from the mirage region to the position sensor.

When z_D is much larger than the confocal distance of the Gaussian probe beam, the phase $\xi\,(x,\ f)$ of the PD signal can be expressed as

$$\xi(x,f) = \varphi - \frac{x}{\mu_{\mathrm{g}}} + \frac{3\pi}{4} + \left(\frac{\omega_1}{2\mu_{\mathrm{g}}}\right)^2. \tag{11}$$

Here φ is the phase shift induced by the sample surface temperature rise and ω_1 the radius of the probe beam at the mirage region. The last term of (11) is the effect of the Gaussian intensity distribution of the probe beam. When $\omega_1 \ll 2\mu_{\mathrm{g}}$, the probe beam may be considered as a 'ray', and this effect may be ignored, as shown in the 'ray theory' of the PD [5]. Our previous experimental study revealed that even though the ratio $\omega_1/(2\mu_{\mathrm{g}})$ was as small as about 0.12, the last term in (11) still played a significant role [16].

For an opaque and thermally thick sample, $|\theta| \approx I_0/\left(2e\sqrt{2\pi f}\right)$ and $\varphi = -\pi/4$. Here I_0 is the excitation laser intensity and e the thermal effusivity of the sample. Equations (10) and (11) then become

$$A(x,f) = \frac{F}{\sqrt{\alpha_{\mathrm{g}}}}\frac{\mathrm{d}n}{\mathrm{d}T}\exp\left(-\sqrt{\frac{\pi f}{\alpha_{\mathrm{g}}}}x\right) \tag{12}$$

and

$$\xi(x,f) = \frac{\pi}{2} + \frac{\omega_1^2}{4}\frac{\pi f}{\alpha_{\mathrm{g}}} - \sqrt{\frac{\pi f}{\alpha_{\mathrm{g}}}}x\,. \tag{13}$$

Here $F = -\gamma I_0 dz_D/(2e)$ is an experimental configuration factor that is a constant and can be measured with a well-known gas, such as pure N_2, as the deflecting medium.

When the deflecting medium is a binary gas mixture, α_{g} and $\mathrm{d}n/\mathrm{d}T$ in (12) and (13) should be replaced by α_{mix} and $(\mathrm{d}n/\mathrm{d}T)_{\mathrm{mix}}$ of the mixture. We have theoretically and experimentally proven that α_{mix} and $(\mathrm{d}n/\mathrm{d}T)_{\mathrm{mix}}$ can be described by a thermal dynamic theory and the Lorentz–Lorenz formula, respectively, providing the theoretical and experimental basis for the predictions of α_{mix} and $(\mathrm{d}n/\mathrm{d}T)_{\mathrm{mix}}$ versus the concentration for a binary gas mixture [16]. According to [16], we have

$$\alpha_{\mathrm{mix}} = \alpha_1\frac{\lambda^{\eta_2}}{1 + [\lambda\,(\alpha_1/\alpha_2) - 1]\,\eta_2} \tag{14}$$

and

$$\left(\frac{\mathrm{d}n}{\mathrm{d}T}\right)_{\mathrm{mix}} = \left(\frac{\mathrm{d}n}{\mathrm{d}T}\right)_1 + \eta_2\left[\left(\frac{\mathrm{d}n}{\mathrm{d}T}\right)_2 - \left(\frac{\mathrm{d}n}{\mathrm{d}T}\right)_1\right]. \tag{15}$$

Here α_1 and α_2 are the thermal diffusivities of gas 1 and gas 2, respectively. $\lambda = k_2/k_1$, where k_1 and k_2 are the thermal conductivities of gas 1 and gas 2, respectively. $(\mathrm{d}n/\mathrm{d}T)_1$ and $(\mathrm{d}n/\mathrm{d}T)_2$ are the temperature coefficients of the refractive indices of gas 1 and gas 2, respectively. Substituting (14) and (15) into (12) and (13), we have

$$\begin{aligned} A(x,f,\eta_2) = {} & \frac{F\sqrt{1 + [\lambda\,(\alpha_1/\alpha_2) - 1]\,\eta_2}}{\sqrt{\alpha_1\lambda^{\eta_2}}} \\ & \times\left\{\left(\frac{\mathrm{d}n}{\mathrm{d}T}\right)_1 + \eta_2\left[\left(\frac{\mathrm{d}n}{\mathrm{d}T}\right)_2 - \left(\frac{\mathrm{d}n}{\mathrm{d}T}\right)_1\right]\right\} \\ & \times\exp\left(-\sqrt{\frac{\pi f\,\{1 + [\lambda\,(\alpha_1/\alpha_2) - 1]\,\eta_2\}}{\alpha_1\lambda^{\eta_2}}}x\right) \end{aligned} \tag{16}$$

and

$$\begin{aligned} \xi(x,f,\eta_2) = {} & \frac{\pi}{2} + \frac{\omega_1^2}{4}\frac{\pi f\,\{1 + [\lambda\,(\alpha_1/\alpha_2) - 1]\,\eta_2\}}{\alpha_1\lambda^{\eta_2}} \\ & - \sqrt{\frac{\pi f\,\{1 + [\lambda\,(\alpha_1/\alpha_2) - 1]\,\eta_2\}}{\alpha_1\lambda^{\eta_2}}}x\,. \end{aligned} \tag{17}$$

In (16) and (17), x and F can be precisely measured [16], and f can be chosen intentionally. With the PD experimental data of the amplitude and phase signals, we can numerically solve (16) and (17) to find the value of the concentration η_2 in mole fraction corresponding to the PD signals. With the concentration values thus obtained, the gas diffusion coefficient D can be determined using (5) or (9).

3 Experiment

3.1 *The Loschmidt cell developed in this work*

Figure 2 shows a Loschmidt diffusion cell developed in this work. It consisted of the top (a) and bottom (b) chambers. The interior length and diameter of each cham-

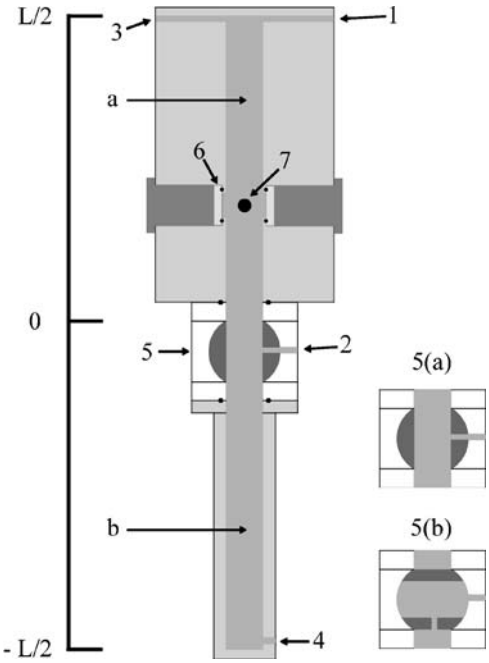

FIGURE 2 A schematic diagram of a diffusion cell. 1: inlet 1 for gas 1; 2: inlet 2 for gas 2; 3 and 4: outlets; 5: a ball valve; 5(a): the ball valve (*open*); 5(b): the ball valve (*closed*); 6: an optical window; 7: a black rubber sample for PD measurements

ber were $0.5L = 177.5$ mm and 20.6 mm, respectively. They could be connected (5(a)) or separated (5(b)) by a ball valve (5) (Apollo 86-104-49). The upper side of the ball valve marked the middle of the diffusion cell ($z = 0$), and the ball valve was part of the bottom chamber. To perform the PD measurement, there were three optical windows (6) on the top chamber to allow the excitation (heating) laser shining on a solid sample and to allow the probe beam traveling through. In the top chamber, there was a small piece of black rubber (7) ($8 \times 8 \times 3$ mm^3) as the solid sample that was positioned at $z = 57.2$ mm. Two mass-flow controllers (Omega, model FMA-5508 0–100 mL/min) were connected to two inlets (1 and 2) to control the gas-flow rate when gases were filled into the chambers.

3.2 *The PD experimental setup*

The diffusion chamber was a part of the setup for the PD measurement. The experimental setup is schematically shown in Fig. 3. After passing through a pupil P, a lens L1, and a mechanical chopper C (EG&G, model 197), the beam of a diode-pumped solid-state laser (Melles Griot, model 58 GLS/GSS 301, 532.0 nm, adjusting the power to 20 mW) hit the black rubber sample in the top chamber uniformly with a diameter $d \approx 6$ mm. The low excitation (heating) power was used to avoid significant dc heating. Parallel to the rubber sample surface at a distance x, a He–Ne probe beam (Melles Griot, model 05LGP 193, 543 nm, 1 mW) was focused by a lens L2 at the mirage region with a waist radius $\omega_0 = (66.0 \pm 0.3)$ μm (see [23] for the method of measuring ω_0) and traveled to a position sensor (ON-TRAK, model OT301), which was connected to a lock-in amplifier (EG&G, model 7260). The whole diffusion cell was mounted on a motorized nano-

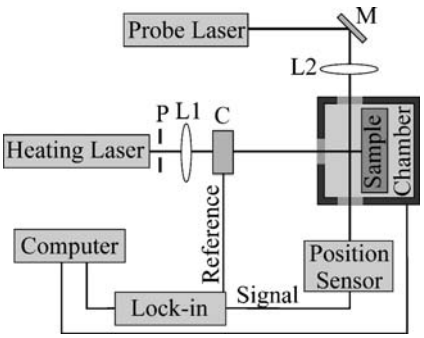

FIGURE 3 A schematic drawing of the experimental setup in the PD measurement. L1 and L2: lenses, C: a mechanical chopper, P: a pupil, M: a mirror

stage (Melles Griot, model 11NCS 101, resolution: 100 nm) for adjusting x. A computer was used to control the lock-in amplifier, chopper, mass-flow controllers, and nanostage with a LabView program. The distance z_D between the mirage region and the position sensor was about 1 m. The distance x was precisely determined as $x = (257 \pm 2)$ mm with the method described in [16, 24]. The experimental configuration factor F in (12) and (16) was measured with pure N_2 as the deflecting medium.

3.3 *The oxygen sensor experimental setup*

An oxygen sensor (Ocean Optics, model FOXY-AL300) was also employed in this work to measure gas diffusion coefficients. Its 300 μm (in diameter) aluminum-jacketed optical fiber probe was installed in the top chamber at the position very close to $z = 0.25L$. On the tip of the optical fiber probe was a ruthenium complex in a sol–gel substrate. The probe was connected to an excitation source and a spectrometer (Ocean Optics, model S2000-FL) by a bifurcated optical fiber. The spectrometer was connected by the computer via a USB A/D converter (Ocean Optics, model ADC 1000). According to the vendor, the response time of the oxygen sensor was around 1 s and the accuracy is 1% of full range for 0%–100% (mole percent).

3.4 *Experimental procedure*

In this work, we measured binary (gas 2–gas 1) diffusion coefficients of CO_2–N_2, CO_2–O_2, N_2–He, O_2–He, CO_2–He, and O_2–N_2. To fill the gases into the diffusion cell, referring to Fig. 2, first, with the inlet 2 and outlet 3 closed and the ball valve opened (5(a)), both chambers (top and bottom) were filled with gas 1 through the inlet 1 for 45 min at a flow rate of 100 mL/min. Meanwhile, the outlet 4 was open to expel the originally existing gas. Second, after both inlet 1 and outlet 4 were closed, the ball valve was closed (5(b)). Third, the bottom chamber was filled with gas 2 through inlet 2 for 30 min at a flow rate of 100 mL/min; at the same time outlet 4 was open to drive out gas 1. Fourth, both inlet 2 and outlet 4 were closed. Finally, both outlet 3 and outlet 4 were opened for around 15 s and then were closed. In this way the pressure inside the diffusion cell was kept at the ambient pressure.

After the gases were filled into the diffusion cell, the PD technique or the oxygen sensor was employed to detect the concentration change of gas 2 in the top chamber. Before the

diffusion started, the PD or oxygen sensor signal was monitored for about 3 min to make sure the system is stable. This signal was also used as a base line. When the ball valve was opened by manually operating the computer, the gas diffusion started, and the concentration of gas 2 in the top chamber began to increase. For each gas mixture, the time-resolved PD signal was recorded for around 1 h and the corresponding time-resolved gas-concentration variation was found by numerically solving (16) and (17), respectively. The oxygen sensor was used to measure O_2 concentration variations for the binary gas mixtures of CO_2–O_2 and O_2–N_2. The concentration variations thus obtained were analyzed with the theoretical diffusion models for long and short times, respectively, to deduce the diffusion coefficients D. The experiment for each binary gas mixture was repeated five times.

4 Results and discussion

4.1 *Gas diffusion*

Equation (5) fully describes the gas diffusion process and shows that the diffusion takes time, which is characterized by the diffusion time τ. Figure 4 shows a theoretical plot of the gas-concentration evolution of gas 2 at the apex ($z = 0.5L$, $L = 355.0$ mm) of the top chamber calculated using (5). The diffusion takes about 2τ to reach the steady state. When $t = \tau$, the concentration of gas 2 is about 0.95 of the concentration of the steady state. The concentration of gas 2 at $z = 0.5L$ is less than 10% of that of the steady state when $t = 0.1\tau$. Consequently, one may consider that when $t < 0.1\tau$, gas 2 has not diffused to the apex ($z = 0.5L$) of the top chamber, and the top chamber can be thought as an infinite space for gas 2 to diffuse in. As a result, for a short time period of $t = 0$ to 0.1τ, (9) can depict the gas diffusion process.

To further examine (9), a theoretical comparison is made between the full diffusion description (5) and the description for short-time diffusion (9), as shown in Fig. 5. In this comparison, the diffusion-cell parameters in this work are used:

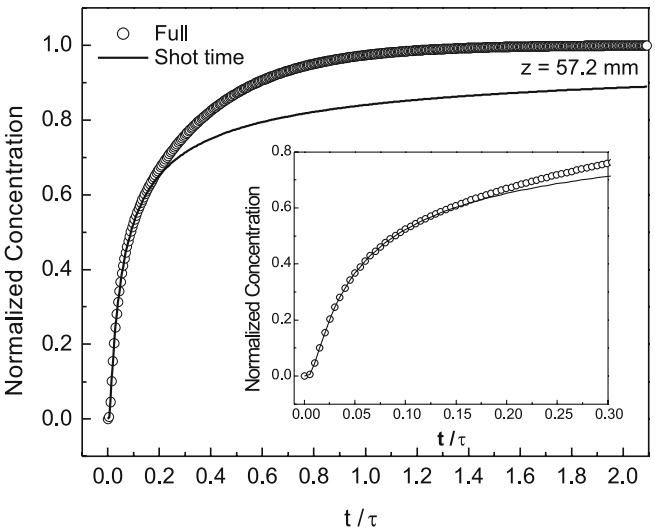

FIGURE 5 A theoretical comparison between (5) and (9). *Circles*: (5), a *solid line*: (9). The scale of the concentration is normalized by the concentration at the steady state. $L = 355$ mm; $z = 57.2$ mm. The *inset* is the detail from $t = 0$ to 0.30τ

$L = 355.0$ mm, and $z = 57.2$ mm, which is the position of the black rubber sample or oxygen sensor in the top chamber. Equation (9) is only consistent with (5) during the early time of the diffusion, as expected. The relative difference between (5) and (9) is about 1% at $t = 0.15\tau$ and 2.6% at $t = 0.2\tau$. Therefore, (9) provides a theoretical basis to process the experimental diffusion data in the early times $t < 0.15\tau$. Moreover, (9) only has one term and is convenient for data processing, such as the least-square curve fitting.

Different from (9), (5) is an infinite series. It is ideal for the data processing if a limited number of terms in (5) is enough to accomplish the task. It is found that there is no difference in using the first 100 terms or 300 terms to numerically calculate (5). The sum of more than 100 terms may be considered enough to represent (5). Equation (5) converges rapidly for

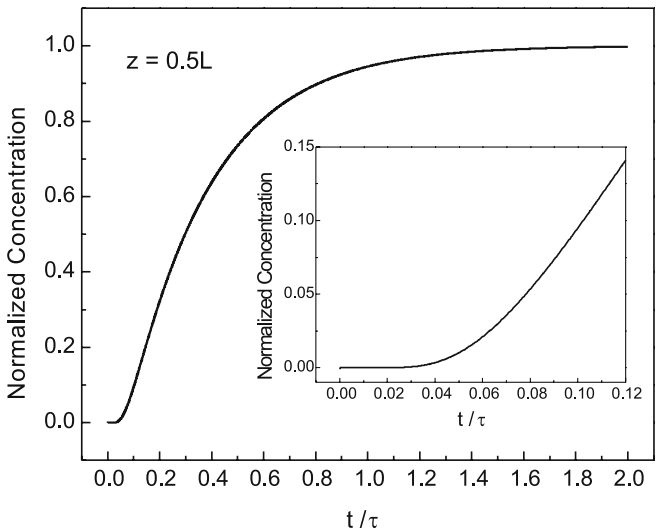

FIGURE 4 A theoretical curve of the gas-concentration evolution at $z = 0.5L$ plotted according to (5). The scale of the concentration is normalized by the concentration at the steady state. $L = 355$ mm. The *inset* is the detail from $t = 0$ to 0.12τ

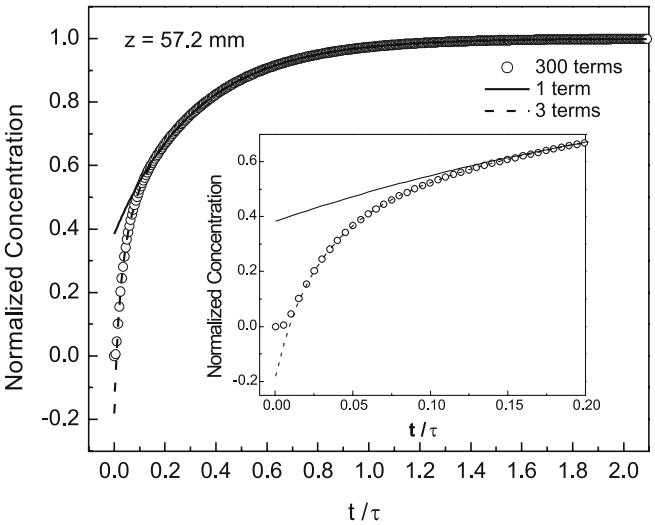

FIGURE 6 Approximations to (5). *Circles*: the sum of 300 terms, a *solid line*: one term, and a *dashed line*: the sum of three terms. The scale of the concentration is normalized by the concentration at the steady state. $L = 355$ mm; $z = 57.2$ mm. The *inset* is the detail from $t = 0$ to 0.20τ

large times. The main difference occurs at the beginning of the diffusion if using fewer terms to approximate (5), as shown in Fig. 6. The relative difference between the first term and the sum of 300 terms is about 5% at $t = 0.1\tau$ and around 1% at 0.15τ. Using the first three terms to approximate (5), the relative difference is less than 1% at $t = 0.025\tau$ and less than 3×10^{-8} at $t = 0.1\tau$. We can conclude that the first three terms are adequate to approximate (5) for $t > 0.1\tau$.

4.2 *Experimental results*

A typical concentration evolution pattern of the gas diffusion measured by the PD technique is shown in Fig. 7 for the binary gas mixture CO_2–O_2. The least-square curve fitting of (9) to the experimental data for a short time and the curve fitting of the first three terms of (5) for a long time are also shown in Fig. 7. In the experiment, the ball valve in Fig. 2 was opened by manually operating the computer, and the exact time t_0 of the beginning of the gas diffusion was unknown. To find t_0, t in (5) and (9) was replaced by $t - t_0$ when curve fittings were performed. In Fig. 7 from $t = t_0 = 221$ s to $t = 521$ s, (9) was fitted to the concentration variations deduced from the PD phase and amplitude signals, resulting in $D = 1.61 \times 10^{-5}\,m^2\,s^{-1}$ and $D = 1.62 \times 10^{-5}\,m^2\,s^{-1}$, respectively, which are consistent with the literature value $D = 1.59 \times 10^{-5}\,m^2\,s^{-1}$ [21]. With $L = 355$ mm and $D = 1.59 \times 10^{-5}\,m^2\,s^{-1}$, the diffusion time $\tau = 2523$ s. The first 300 s ($t - t_0 = 300$ s) is about $0.12\tau < 0.15\tau$, and (9) fitted the concentration variation well with the same correlation coefficient $R > 0.994$ for both of the foregoing fitting results. From 720 s to 3800 s, (5) was fitted to the concentration curves deduced from the PD phase and amplitude signals with $R > 0.983$ and $R > 0.984$, respectively, and the diffusion coefficient D was found to be $1.64 \times 10^{-5}\,m^2\,s^{-1}$ and $1.7 \times 10^{-5}\,m^2\,s^{-1}$, respectively. These experimental results confirm the discovery discussed in Sect. 4.1.

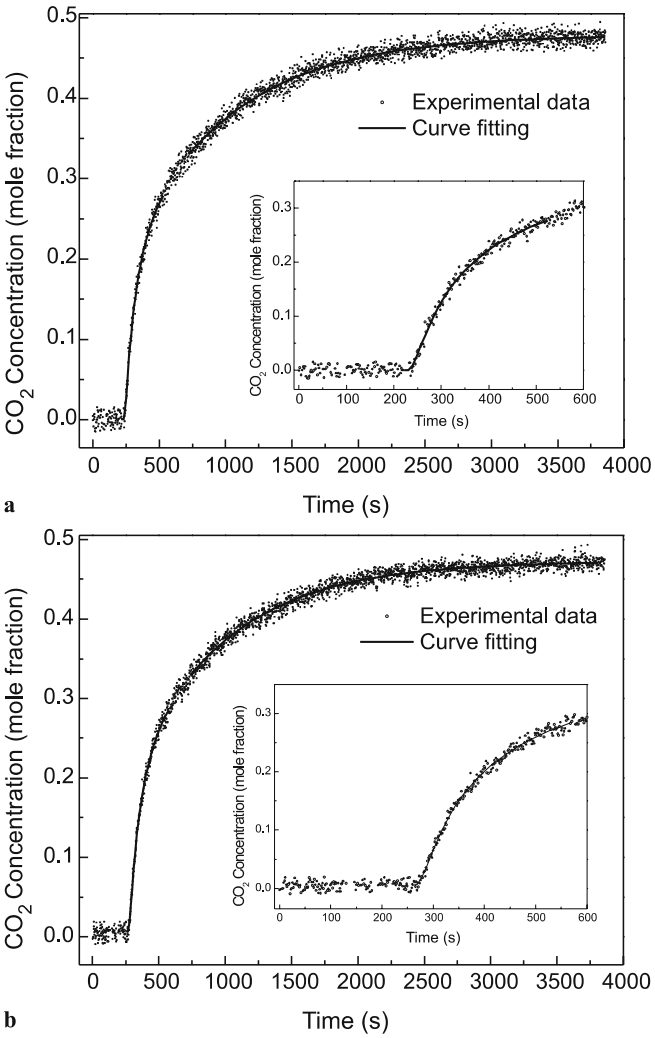

FIGURE 7 The concentration evolution of CO_2 in a binary gas mixture of CO_2–O_2 measured by the PD technique and the curve fittings of (5) and (9) to the concentration variation. The *inset* is the detail from $t = 0$ to 600 s. (**a**) Measured by PD phase signal, (**b**) measured by PD amplitude. *Small circles*: experimental data, *solid lines*: curve fittings to (9) and the first three terms of (5), respectively. $L = 355$ mm; $z = 57.2$ mm

Figure 7 shows one measurement, and all the results of the binary diffusion coefficients measured with the PD technique are shown in Tables 1 and 2, in which the binary gas mixtures are written in the order of gas 2–gas 1. Recall that in the experiment the gas 1 was in the top chamber before the diffusion started and dominated the deflecting medium in the early stage of the diffusion. For the gas mixtures of gas 2–He, the PD signals were small in the early stages (short times), because of the high thermal diffusivity of He. Consequently, the PD phase signals and the binary coefficients could not be measured. Overall, the measured values of D are well consistent with the literature ones, and their relative differences are within 10%, except for CO_2–N_2 with the long-time PD amplitude measurement. Examining Tables 1 and 2, one may find that the relative differences for the measured values of D deduced from the phase signals are smaller than those from the amplitude signals. The benefit with the phase signal can be attributed to the immunization of the phase signal to the

Gas mixture	D measured (short time)	D measured (long time)	D literature
CO_2–He		5.3 ± 0.1	5.13
N_2–He		6.3 ± 0.2	6.98
O_2–He		6.4 ± 0.2	6.97
CO_2–N_2	1.68 ± 0.03	1.65 ± 0.03	1.60
CO_2–O_2	1.60 ± 0.03	1.60 ± 0.04	1.59

The literature values of D are quoted from [21]

TABLE 1 The binary diffusion coefficients ($\times 10^{-5}\,m^2\,s^{-1}$) of various gas mixtures measured with PD phase signals

Gas mixture	D measured (short time)	D measured (long time)	D literature
CO_2–He	5.5 ± 0.2	5.5 ± 0.2	5.13
N_2–He	7.2 ± 0.1	6.4 ± 0.1	6.98
O_2–He	7.3 ± 0.1	6.4	6.97
CO_2–N_2	1.70 ± 0.04	1.8 ± 0.2	1.60
CO_2–O_2	1.62 ± 0.03	1.5 ± 0.2	1.59

The literature values of D are quoted from [21]

TABLE 2 The binary diffusion coefficients ($\times 10^{-5}\,m^2\,s^{-1}$) of various gas mixtures measured with PD amplitude signals

fluctuation of the excitation laser power. Also, the short-time measurements are better than the long-time ones, especially for the amplitude measurements, probably due to the fact that the excitation laser has a long time power stability of 3%.

In terms of the precision of the measurements with the PD technique, all the standard deviations are less than 3.2% of the averaged D values with the phase measurements. Regarding the PD amplitude measurements, the highest ratio of the standard deviation over the averaged D is 3.6% for the short-time measurements, and 13% for the long-time measurements, indicating that high precision can be achieved using the PD technique with the short-time measurement.

In this work the concentration dependences of α_{mix} and $(\mathrm{d}n/\mathrm{d}T)_{\mathrm{mix}}$ were utilized to measure the concentration evolution of gas 2 in the top chamber and then the diffusion coefficients of binary gas mixtures. The larger the differences of the thermal diffusivities and the temperature coefficients of the refractive index between gas 2 and gas 1, the more sensitive this method is for measuring the concentration variation. Besides the PD technique, some photothermal techniques can measure the thermal diffusivities of gases [2], such as a thermal wave interferometer [17], namely a thermal wave resonant cavity technique [25]. Lima et al. [17] measured binary diffusion coefficients of hydrocarbon (i.e. n-pentane, n-hexane, and n-heptane) vapors in air using a thermal wave interferometer. An open container with a liquid-hydrocarbon sample inside was placed under the interferometer. The concentration evolution of the hydrocarbon in air was monitored by measuring the temporal change of the thermal diffusivity of the hydrocarbon–air mixture. The diffusion coefficient was calculated with the measured concentration variation using a theoretical diffusion model. Three significant figures of the diffusion coefficients were obtained, which was the same as that of this work. In their work, only thermal diffusivity was used to evaluate the temporal concentration variation, and the adequate difference of the thermal diffusivities between the vapor and air was required for a sufficient sensitivity to measure the thermal diffusivity variation. Our method in this work has the same requirement if using the phase signal only. Fortunately, the PD amplitude signal is linearly proportional to the temperature coefficient of the refractive index of the deflecting medium, which is concentration dependent. If the values of $\mathrm{d}n/\mathrm{d}T$ of gas 2 and gas 1 are sufficiently different, the concentration evolution can be measured, even though the thermal diffusivities of the gases are similar. In comparison with the thermal wave interferometer, the PD technique presented in this work has broader applications in terms of the determination of diffusion coefficients of binary gas mixtures.

Besides the PD technique, an oxygen sensor was also used in this work to measure the binary diffusion coefficients of CO_2–O_2 and O_2–N_2. Compared with the PD concentration measurements shown in Fig. 7, the O_2 concentration evolution measured by the oxygen sensor in the mixture of O_2–N_2, shown in Fig. 8, has less noise. Table 3 shows the results of the diffusion coefficients measured by means of the oxygen sensor. The measured D of the mixture of CO_2–O_2 has smaller deviation, i.e. 0.6% of the mean, compared with 1.9% and 2.5% with the PD phase measurements for short and long times, respectively. However, our experimental results exhibit that the oxygen sensor only works fine for the long-time

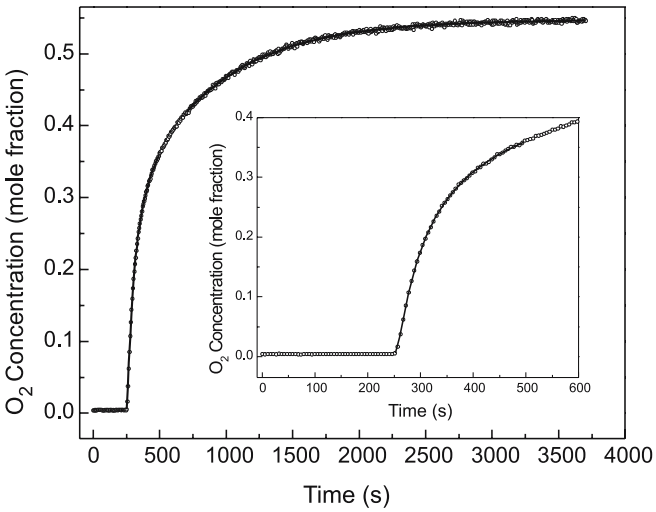

FIGURE 8 The concentration evolution of O_2 in a binary gas mixture of O_2–N_2 measured by the oxygen sensor and the curve fittings of (5) and (9) to the concentration variation. The *inset* is the detail from $t = 0$ to 600 s. *Small circles*: experimental data, *solid lines*: curve fittings to (9) and the first three terms of (5), respectively. $L = 355$ mm; $z = 57.2$ mm

Gas mixture	D measured (short time)	D measured (long time)	D literature
O_2–N_2	2.99 ± 0.01	1.98 ± 0.03	2.02
CO_2–O_2	2.06 ± 0.03	1.58 ± 0.01	1.59

The literature values of D are quoted from [21]

TABLE 3 The binary diffusion coefficients ($\times 10^{-5}$ m^2 s^{-1}) of two gas mixtures with O_2 measured with the oxygen sensor

measurements. Table 3 displays that the values of D obtained from the short-time measurements deviate far away from the literature ones. Considering that the time scale of the short-time measurement is about 200 s, the sensor responding time, which is about 1 s, should not be a significant problem for the short-time measurement. The calibration procedure could be a reason for the failure of the short-time measurement. According to the manual of the sensor, the sensor needs a calibration with three oxygen concentrations, such as 0%, 50%, and 100%, for the whole measurement range of the sensor. For the short-time measurement of O_2–N_2, the oxygen concentration was low; in contrast, for the short-time measurement of CO_2–O_2 the oxygen concentration was high. The sensor seemed not able to measure the concentration correctly in either case with the three-point calibration and seemed to work well in the middle area. A calibration with more points or a calibration for a narrower concentration range may be required for the oxygen sensor. A full investigation is ongoing. Besides the calibration problem, a long-term (1–2 weeks) degradation of the sensor exists, which leads to the requirement of frequent calibrations.

5 Conclusions

In this work, the photothermal deflection technique was successfully applied in the measurements of the binary diffusion coefficients of various gas mixtures based on our previous theoretical and experimental studies [3, 16, 24]. With

two theoretical mass-diffusion models and the characteristic diffusion time $\tau = L^2/(\pi D)$ explored in this work, we measured the gas-concentration evolution in an in-house-made Loschmidt diffusion cell by either the PD technique or a fiber optic oxygen sensor. Experimental results showed that the binary diffusion coefficients could be determined precisely using the PD technique, especially using the PD phase signals. Compared with the oxygen sensor, the PD technique has advantages in the binary diffusion coefficient measurements:

1. The PD technique can be applied to measure a variety of gas mixtures; on the contrary, the oxygen sensor can only be employed to measure the gas mixtures with oxygen.
2. The PD technique is suitable for both short- and long-time measurements, while the oxygen sensor is only suitable for the long-time measurements.
3. Unlike the oxygen sensor, the PD technique has no issue of degradation. The technique and apparatus developed in this work can be applied to measure the effective diffusion coefficients of porous materials.

REFERENCES

1 D. Almond, P. Patel, *Photothermal Science and Techniques* (Chapman & Hall, London, 1996)
2 H. Vargas, L.M.C. Miranda, Rev. Sci. Instrum. **74**, 794 (2003)
3 J. Zhao, J. Shen, C. Hu, Opt. Lett. **27**, 1755 (2002)
4 A.C. Boccara, D. Fournier, J. Bades, Appl. Phys. Lett. **36**, 130 (1980)
5 J.P. Roger, F. Lepoutre, D. Fournier, A.C. Boccara, Thin Solid Films **155**, 165 (1987)
6 M. Bertolotti, R. Li Voti, G. Liakhou, C. Sibilia, Rev. Sci. Instrum. **64**, 1576 (1993)
7 M. Bertolotti, S. Ligia, G. Liakhou, R. Li Voti, S. Paoloni, C. Sibilia, J. Appl. Phys. **85**, 2881 (1999)
8 J.F. Power, S.W. Fu, M.A. Schweitzer, Appl. Spectrosc. **54**, 110 (2000)
9 J. Zhou, J. Zhao, J. Shen, M.L. Baesso, J. Opt. Soc. Am. B **22**, 2409 (2005)
10 D. Fournier, A.C. Boccara, N.M. Amer, R. Gerlach, Appl. Phys. Lett. **37**, 519 (1980)
11 B.L. Zimering, A.C. Boccara, Appl. Opt. **36**, 3188 (1997)
12 S.N. Nickolaisen, S.E. Bialkowski, J. Chromatogr. **366**, 127 (1986)
13 G. Liakhou, S. Paoloni, M. Bertolotti, J. Appl. Phys. **96**, 4219 (2004)
14 J.C. Loulergue, A.C. Tam, Appl. Phys. Lett. **46**, 457 (1985)
15 A. Salazar, A. Sánchez-Lavega, Rev. Sci. Instrum. **70**, 98 (1999)
16 J.H. Rohling, J. Shen, J. Zhou, C.E. Gu, A.N. Medina, M.L. Baesso, J. Appl. Phys. **99**, 103 107 (2006)
17 J.A.P. Lima, M.G. da Silva, M.S. O Massunaga, E. Marín, L.C.M. Miranda, J. Appl. Phys. **91**, 5581 (2002)
18 N. Matsunaga, M. Hori, A. Nagashima, High Temp. **30**, 77 (1998)
19 F.R.W. McCourt, D. Weir, G.B. Clark, M. Thachuk, Mol. Phys. **103**, 17 (2005)
20 J. Baranski, E. Bich, E. Vogel, J.K. Lehmann, Int. J. Thermophys. **24**, 1207 (2003)
21 T.R. Marrero, E.A. Mason, J. Phys. Chem. Ref. Data **1**, 3 (1972)
22 J. Crank, *The Mathematics of Diffusion*, 2nd edn. (Oxford University Press, New York, 1975)
23 J. Shen, R.D. Lowe, R.D. Snook, Chem. Phys. **165**, 385 (1992)
24 J.H. Rohling, J. Shen, J. Zhou, C.E. Gu, Opt. Lett. **31**, 44 (2006)
25 J. Shen, A. Mandelis, T. Ashe, Int. J. Thermophys. **19**, 579 (1998)